

CONSTRAINTS ON LITHOSPHERIC STRUCTURES OF THE EASTERN ALPS FROM GRAVIMETRY

Mitterbauer, U.; Brückl, E.; Behm, M.; CELEBRATION 2000 & ALP 2002 Working Group
 Institute of Geodesy and Geophysics, Vienna University of Technology

3D Seismic Model of the Eastern Alps derived from CELEBRATION 2000 and ALP 2002 Data

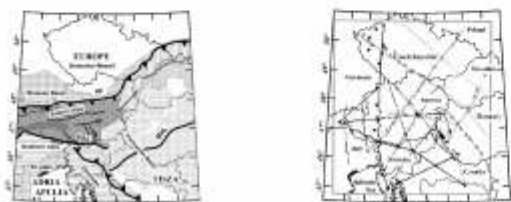


Figure 1: Tectonic setting of the investigation area.



Figure 2: Field layout of CELEBRATION 2000, 3rd deployment (grey) and ALP 2002 (black). Shots are shown as triangles, receivers as dots.

The Eastern Alps and their transition to the surrounding tectonic provinces (Bohemian Massif, Carpathians, Pannonian domain and Dinarides) include the transition from the head on collision between the European and the Adriatic-Apulian plates in the central part of the Eastern Alps, the extrusion of the eastern part into the Pannonian domain and the transition of the Eastern Alps to the Dinarides (Figure 1). This area was investigated by two recent 3D seismic refraction experiments in Central Europe, CELEBRATION 2000 and ALP 2002. Data from the 3rd deployment of CELEBRATION 2000 (55 shots, 844 receivers and a total profile length of 2 800 km) and ALP 2002 (39 shots, 947 receivers and a total profile length of 4 300 km) has been merged (Figure 2). A 3D velocity model of the P-wave velocity structure of the crust and the Moho discontinuity has been derived from Pg-diving wave tomography (Figures 3a-c), Pn-delay time decomposition and PmP-wide angle reflections. (Figures 4 and 5).

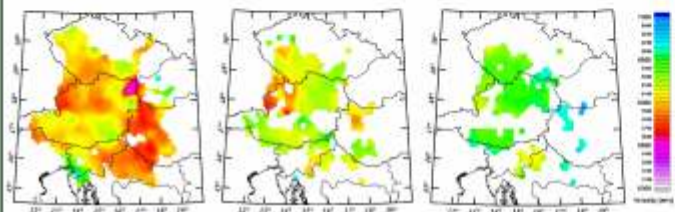


Figure 3: Depth slices through the 3D P-wave velocity model of the crust in (a) 7 km, (b) 14 km, and (c) 21 km depth.

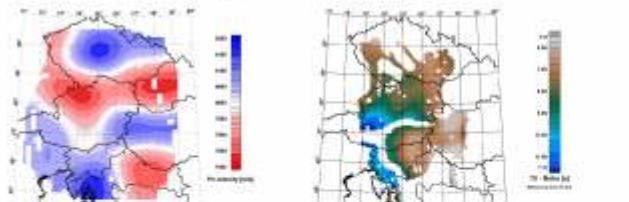


Figure 4: Pn-velocity

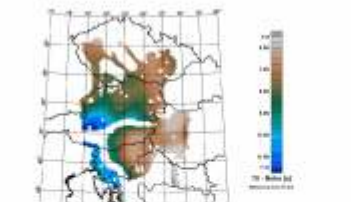


Figure 5: Vertical (migrated) 2-way Moho reflection travel time T_0 ; reference datum $Z = 10$ km.

Incomplete Velocity Information about the Lower Crust

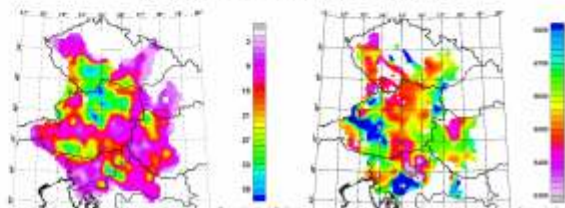


Figure 6: Penetration depth of Pg-diving wave tomography.

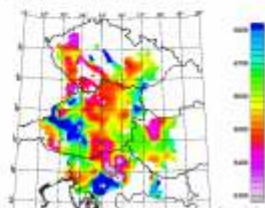


Figure 7: Preliminary model of the average P-wave velocity of the crust between $Z = 10$ km and the Moho.

The velocity information about the crust is not complete, since in most areas the diving wave tomography does not penetrate down to the Moho (Figure 6). A preliminary model of the average P-wave velocity of the crust between $Z = 10$ km and the Moho was constructed by estimating the P-wave velocity between the maximum penetration depth and the Moho from V_{m0} velocities derived from a PmP-velocity analysis. Furthermore, constraints from global (Christensen and Mooney, 1995) data were used in order to exclude unreasonable interval velocities.

Additional Constraints from Gravity and Isostatic Equilibrium

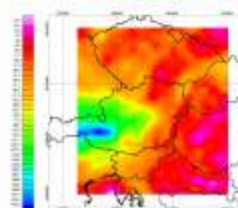


Figure 8: Bouguer gravity map of the investigation area compiled from 'New Austrian Bouguer Map' (Kraiger and Köhntreiber) and WEGEP data.

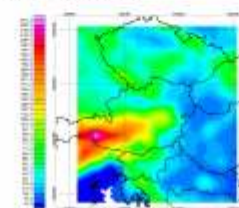


Figure 9: Smoothed surface elevation model of the investigation area.

Additional constraints on the velocity of the lower crust (below the penetration depth of the diving wave tomography) can be derived from gravity and isostasy assuming a definite relation between P-wave velocity and density. The **Christensen and Mooney velocity-density relationship** (1995) will be used consequently for this study. The gravity modelling will be done by a superposition of the gravity effects of prismatic bodies after Nagy (1966). Densities relative to a reference model will be used in order to avoid edge effects.

Determination of an Average Linear Velocity Function of the Lower Crust

$$V_p(Z) = 6.08 \text{ km s}^{-1} + (Z - 10 \text{ km}) 0.027 \text{ s}^{-1}$$

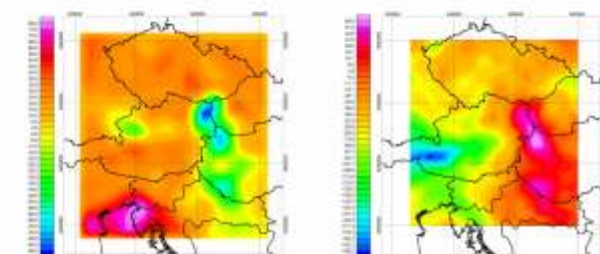


Figure 10: Gravity effect of the upper crust ($Z \leq 10$ km).

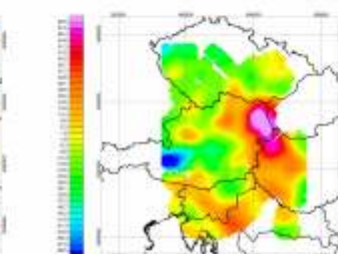


Figure 11: Residual gravity after stripping the effect of the upper crust ($Z \leq 10$ km).

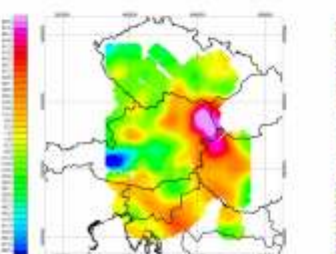


Figure 12: Residual gravity after subtracting the effect of the lower crust with an average linear velocity function.

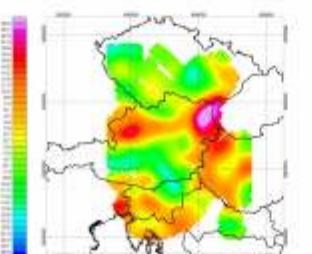


Figure 13: Vertical normal stress at $Z = 55$ km calculating the effect of the lower crust with an average linear velocity function.

Between surface and the level $Z = 10$ km the 3D P-wave velocity model is nearly complete. Therefore, the conversion to densities and the calculation of the gravity effect (Figure 10) is straight forward. Subtraction of this gravity effect from the Bouguer anomaly yields a residual gravity which still shows the effect of the varying depth of the Moho, but also compensating masses below sedimentary basins, especially the Vienna basin (Figure 11).

The next step is the estimation of an average linear velocity function of the lower crust (below $Z = 10$ km). This function has been found by minimizing the correlations between the migrated 2-way Moho reflection travel times with the residual gravity (Figures 5 and 12) and the vertical normal stress at $Z = 55$ km (Figure 13). The obtained velocity function $V_p(Z) = 6.08 \text{ km s}^{-1} + (Z - 10 \text{ km}) 0.027 \text{ s}^{-1}$ is in good agreement with the results of Christensen and Mooney (1995) for the mean crust. A density of $3 250 \text{ kg m}^{-3}$ has been assumed for the uppermost mantle. The residual gravity (Figure 12) can be related to tectonic and geodynamic structures. Evidence for a "Dinaric subduction" is indicated by positive anomalies. Strong positive anomalies are also found in the transition from the Northern Pannonian domain to the European platform, where high velocities in the lower crust are obtained from the seismic model. Negative anomalies can be correlated with the South Bohemian Pluton and the Tauern Window. The distribution of the vertical normal stress at $Z = 55$ km shows a corresponding pattern (Figure 13).

Depth of Sources for Residual Gravity and Deviation from Isostatic Equilibrium

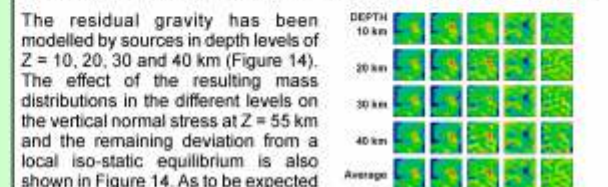


Figure 14: Modeling of residual gravity by sources at different levels. Columns (1) observed gravity residual; (2) calculated gravity residual; (3) sources of residual gravity (surface densities); (4) variation of normal stress at $Z = 55$ km for average lower crust; (5) variation of normal stress at $Z = 55$ km, effect of residual gravity sources added. Rows 1 - 5 sources of residual gravity in $Z = 10, 20, 30, 40$ km and average.

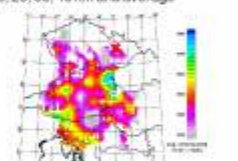


Figure 15: Average P-wave velocity of the crust between $Z = 10$ km and the Moho derived from gravimetric data.

RESULT: Combination of Seismic and Gravimetric Velocity Information

Figure 16 shows the ratio V_{seis}/V_{grav} versus the ratio of penetration depth to crustal thickness R . It is evident, the greater the penetration depth of the diving wave tomography, the less is the deviation of the ratio V_{seis}/V_{grav} from unity. We therefore construct a velocity solution from a weighted mean of V_{seis} and V_{grav} seismic solution: $V_{seis+grav} = R V_{seis} + (1-R) V_{grav}$ (Figure 17). Because of the weighting scheme, the seismic information about the lower crust is not changed where information from diving wave tomography is available. Figure 18 shows the reflection time map of the Moho (Figure 5) converted to depth by the use of the combined seismic-gravimetric velocity model of the lower crust.

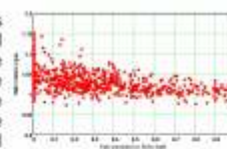


Figure 16: Ratio V_{seis}/V_{grav} versus the ratio of penetration depth to crustal thickness.

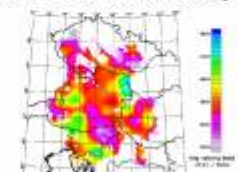


Figure 17: Average P-wave velocity of the crust between $Z = 10$ km and the Moho combined from seismic and gravimetric data.



Figure 18: Moho depth map calculated by the use of the combined seismic-gravimetric velocity model of the lower crust.

CELEBRATION 2000 & ALP 2002 WORKING GROUP



References:

Christensen, N.I. and W.D. Mooney, 1995, Seismic velocity structure and composition of the continental crust: A global view, *J. Geophys. Res.*, 100, 9761-9788.
 Nagy, D., 1996, The gravitational attraction of right angular prism, *Geophysics* 31, pp. 352-371.

Acknowledgement:

This study has been granted by the Austrian Academy of Sciences and Austrian Science Fund (FWF)

